Aerosol Science and Technology

A Linear Trap for Studying the Interaction of Nanoparticles with Supersaturated Vapors

Denis Duft[a], Mario Nachbar[b], Markus Eritt[b] & Thomas Leisner[ab]

[a] Institute for Meteorology and Climate Research - Atmospheric Aerosol Research (IMK-AAF), Karlsruhe Institute of Technology (KIT), Karlsruhe, Germany

[b] Institute of Environmental Physics (IUP), Ruprecht-Karls-University Heidelberg, Heidelberg, Germany
Accepted author version posted online: 19 Jun 2015.

CrossMark

Click for updates

PLEASE SCROLL DOWN FOR ARTICLE

THE MOLECULAR FLOW ICE CELL - MICE

A Linear Trap for Studying the Interaction of Nanoparticles with Supersaturated Vapors

Denis Duft[1,*], Mario Nachbar[2], Markus Eritt[2,‡] Thomas Leisner[1,2]

[1]*Institute for Meteorology and Climate Research - Atmospheric Aerosol Research (IMK-AAF), Karlsruhe Institute of Technology (KIT), Karlsruhe, Germany*

[2]*Institute of Environmental Physics (IUP), Ruprecht-Karls-University Heidelberg, Heidelberg, Germany*

‡*present address:* Integrated Carbon Observation System (ICOS)*, Max Planck Institute for Biogeochemistry, Jena, Germany*

Address correspondence to Denis Duft, Institute for Meteorology and Climate Research - Atmospheric Aerosol Research (IMK-AAF), Karlsruhe Institute of Technology (KIT), P.O. Box 3640, Karlsruhe 76021, Germany. E-mail: denis.duft@kit.edu

Abstract

We present and characterize a versatile device for studying the controlled interaction of free nanoparticles with supersaturated vapors. It utilizes a rf- ion trap for storing a cloud ($>10^8$ particles) of singly charged nanoparticles in the sub 10 nm size regime and combines it with a static supersaturation chamber operating at low pressure in the free molecular flow regime. This allows for the stable production of a homogeneous zone of variable saturation that can reach very high levels of supersaturation ($S>10^4$). Compared to diffusion chambers, much higher saturations and more homogeneous saturation fields can be achieved and convective flow is not an issue.

The analysis of the adsorption and nucleation processes on the surface of the nanoparticles can be performed by mass spectrometry and optical spectroscopy. We discuss the general function principle of the device and demonstrate that it is well suited for studying water adsorption and deposition ice nucleation on metal oxide nanoparticles under conditions of the upper atmosphere of the Earth and of Mars.

1.   Introduction

Nanoparticles bridge the gap between atoms and atomic clusters and condensed matter. Due to their specific and size dependent properties, they have found widespread application in science and technology but also play an important role in many natural processes. In atmospheres, they act as condensation nuclei for vapors to promote the formation of the liquid or solid phase. During the last decades, substantial progress has been made in cluster and nanoparticle research by applying vacuum techniques like electron microscopy (Liu 2005; van der Veen, Kwon et al. 2013), mass spectrometry (Wang and Johnston 2006; Murphy 2007; Zordan, Pennington et al. 2010) and x-ray photoelectron spectroscopy (Wu, Yin et al. 2006; Wilson, Shengli et al. 2007; Meinen, Khasminskaya et al. 2010; Antonsson, Bresch et al. 2013). These techniques allow assessing the interplay between the electronic and geometric structure of the particles and their chemical and optical properties. This progress is made however at the cost of removing the particles from their natural or technological environment with the risk of altering their properties in that process. Therefore, newer techniques like environmental scanning electron microscopy (Nishiyama, Koizumi et al. 2014), high pressure photoelectron spectroscopy (Bluhm, Andersson et al. 2006; Salmeron and Schlögl 2008; Mysak, Starr et al. 2010) try to extend the modern technologies to more realistic atmospheric conditions.

In the line of this approach, we describe in this contribution the design and characterize the performance of a novel type of ion trap for singly or weakly charged nanoparticles. This device allows exposing freely levitated nanoparticles to supersaturated vapors for studying the nucleation and growths of the condensed phase on these particles. A typical, but not the only area of application of such a device is the nucleation of ice particles in planetary atmospheres at low

temperatures as occurring in the nucleation of mesospheric ice clouds in the polar summer mesopause of the Earth (Rapp and Thomas 2006; Gumbel and Megner 2009). The notion of ice in this context is not restricted to H_2O ice but may refer to any solid formed from a condensable vapor (e. g. CO_2, Hydrocarbons etc.).

This device, which we call the molecular flow ice cell (MICE), is an extension to our apparatus TRAPS (Trapped Reactive Atmospheric Particle Spectrometer), that was described previously (Meinen, Khasminskaya et al. 2010). It allows to expose a large ($>10^8$ particles) and well characterized ensemble of sub 10nm dia. nanoparticles to condensable vapors of well-defined and variable saturation including high supersaturation. The principle of operation of this novel device is similar to the well-known diffusion chamber. There are two fundamental differences however. In MICE, we cannot employ the simple co-planar or concentric geometry typically found in diffusion chambers but we have to retain the symmetry of the linear quadrupole ion trap. More importantly, the background gas pressure in the nanoparticle trap is low. Therefore MICE does not operate in the continuous flow regime, where diffusion controls the concentrations of the vapor but in the free molecular regime. As it is detailed below, this greatly facilitates the creation of high levels of supersaturation.

This manuscript is organized as follows: In section 2 we provide the underlying principles of MICE, while in section 3 we describe the actual design of the new ice cell in detail. In section 4, we show representative measurements of the adsorption of water on metal oxide particles and the heterogeneous nucleation of ice on the surface of these particles in order to demonstrate the proper operation of MICE. In section 5 we discuss possible applications and limitations of the device.

2. Principle of operation

The diffusion chamber was introduced by Langsdorf (1939) as a device to create a stationary and well-controlled volume of supersaturated vapor. In its most simple form, it consists of two large parallel plates held at close distance to each other. The opposing surfaces are coated with the condensed phase of the species of interest and are kept at disparate temperatures. If the transport of heat and vapor from the warm to the cold plate is governed by diffusion, an approximately linear gradient of both parameters is established in the space between the plates (Brown Jr and Schowengerdt 1979).

A schematic representation of this situation is given in Fig. 1a, which illustrates that the highly nonlinear dependence of vapor pressure on temperature gives rise to a central zone of supersaturation. The diffusion chamber principle is not limited to the coplanar geometry depicted above and other geometrical arrangements, like e.g. concentric cylinders have been employed (Severynse 1964; Saxena and Carstens 1971; Rogers 1988). It may be extended to arbitrary geometries by applying the stationary diffusion equation for temperature and vapor in that geometry. If however the device is operated in the regime of free molecular flow, i.e. if the mean free path in the gas phase is larger than the distance between the plates, this situation changes. Under these conditions, the molecules evaporating from each wall retain their Maxwellian velocity distribution corresponding to the temperature of that wall. The particle temperature and the concentration of vapor molecules at any point in space can be calculated in a straightforward way to be the arithmetic average of the temperatures and saturation concentration of the walls weighted with the solid angle fraction under which each wall is seen by the particle (for details see appendix). In the case of two parallel plates, the respective high temperature- and low

temperature- weighting fractions are constants of ½ and independent of position. This situation is depicted in Fig. 1b. As exemplified for the actual geometry of MICE below, the supersaturation under free molecular flow conditions is generally higher and spatially more extended than in the diffusion limited case.

3. Design of the ice cell

MICE is a part of the TRAPS apparatus (Meinen, Khasminskaya et al. 2010), which is sketched in Fig. 2 and which is only briefly recalled here. It consists of an high intensity source for singly charged small nanoparticles (1), an aerodynamic lens (2) optimized to focus these nanoparticles into an vacuum- apparatus, an ion guide (3) to moderate and precool the particles, two quadrupole deflectors (4) and (5) to introduce and extract the particles from a temperature-variable linear nanoparticle trap (6) and a time-of-flight nanoparticle mass spectrometer (7) to analyze the mass of the particles after extraction.

MICE replaces the linear nanoparticle trap (6). It combines an ion trap with a supersaturation chamber and its geometry is depicted in Fig. 3. The ion trap (r_0=7 mm) is made of four parallel gold plated copper rods (length 480 mm) with semi-circular cross-section (d=16 mm) in a quadratic arrangement, to which the rf-AC potentials are applied. The potential on these rods creates the trapping fields for the particle containment. The rods are mounted inside a copper tube using SHAPAL[1] ceramic spacers as electrical-insulators providing a high thermal conductivity. This assembly is mounted to a He- closed cycle cryostat (DE-104B-Turbo, Advanced Research Systems, Inc.) and serves as the cold wall in our setup. Under typical static

---

[1] ™Tokuyama Corp, Tokyo, JP

operation conditions, we measured the maximum temperature difference between the outer tube and the quadrupole rods (kept at ground potential) to be below 0.1 K.

Radially located between the cooling tube and the quadrupole rods, is an additional tube made of gold plated copper, which has openings at the angular positions of the quadrupole electrodes but covers the space between them. It is kept at electric ground potential and acts as the warm wall in our setup. Therefore it is mounted to the outer tube using PEEK[2] spacers which feature a very low thermal conductivity. The warm wall is heated using two heating foils located in an optimized position to minimize temperature gradients along the element. Six calibrated PT100 temperature sensors are placed in small cavities along its longitudinal coordinate. One of the sensors is used for temperature regulation while the remaining five are used for temperature monitoring.

In order to produce supersaturation, the warm and cold walls have to be covered with a layer of the condensable substance while being held at a low temperature. To deposit this layer prior to an experiment, a hollow stainless steel tube extending over the full length of MICE may be inserted via a feedthrough on the central axis (Fig. 3 (8)). The tube is closed on the far end and is connected to the vapor of the condensate at the other end. It carries four rows of laser drilled holes along its linear axis. Each row consists of one hundred holes with a diameter of 100 µm and 5 mm spacing between each hole such that the length of the particle trap is covered. The rows are located at angles of ninety-degrees in the direction of the warm wall, in order to direct the vapor exiting through the holes preferentially to the inner surface of the warm wall, as

---

[2]™Victrex plc. Lancashire, UK

indicated by the arrows in Fig. 3a. At typical vapor pressure inside the tube of several hPa, the deposition is conducted for about 10 minutes to yield a typical layer thickness of several 10µm.

For the chosen geometry, the temperature and vapor concentration profiles cannot be calculated analytically as compared to the idealized geometry discussed in the previous section. The diffusion equation has been solved numerically and the geometrical warm and cold wall weighting fractions have been calculated as a function of position.

In Fig. 4 we compare the calculated temperature distribution and supersaturation profile both for diffusive (Fig. 4a) and free molecular flow (Fig. 4b) using the established parameterization for the saturation vapor pressure over Ice Ih from Murphy and Koop (2005). The lower panels show a central cross section of the temperature and saturation profiles along the horizontal dashed line. As noted above, the supersaturation under free molecular flow condition reaches higher values and extends over a larger volume than in the diffusive case. In both cases, the profiles are sufficiently flat to ensure homogeneous conditions for the particles which are stored in the particle trap. The radial particle density distribution in a gas filled linear quadrupole trap has been measured and calculated previously (Majima, Santambrogio et al. 2012). From their results one can estimate that under typical operation conditions (V_{rf}=800 V, Ω=2π·50 kHz, m=1.2·10^5 u, q=+1e) and a well filled particle trap (N=10^8) the ion cloud is radially confined to within a radius of 1mm around the central axis of the ion trap (indicated by a red dashed line in Fig. 4).

Close to the ends of the particle trap, the temperature- and saturation profiles are no longer constant, as the ion lenses at the entrance and exit of the MICE are kept on the cold wall temperature. This does not introduce much inhomogeneity, as illustrated by the warm surface weighting function F_w (c.f. appendix) which is given along the central axis in Fig. 5. A zone of

reduced F_w and thus reduced supersaturation extends to about 10 % of the total length of the trap into each end of the trap. Fortunately, the end electrodes repel the particles, so that this zone is also a zone of reduced particle density (c.f. Fig. 5, dashed line).

4.   Experiments

The setup presented above has been characterized in a series of experiments using nanoparticles of various metal oxides and both water and carbon dioxide vapors. All experiments were performed at low temperatures between 80 K and 150 K where the corresponding vapor pressure is low enough to obtain a stable operation of the trap and the deposit of solid phase on the warm walls is depleted at a rate low enough to be compatible with several hours of operation of MICE. The trap is operated at a background of Helium gas of about 0.2 Pa. Under these conditions, Helium atoms are much more abundant than vapor molecules. This ensures that the temperature of the nanoparticles and the wall surfaces is not influenced by the latent heat associated with evaporation- and condensation processes. At the same time, the density of helium atoms is still low enough to operate the trap in the regime of free molecular flow (c.f. discussion of Fig. 10 below), which allows for a higher and more homogeneous supersaturation to be applied.

A typical MICE-TRAPS experiment starts by cooling MICE to a temperature well below the lowest temperature to be applied to the cold wall. Under these conditions, the condensed phase of the material under investigation is frozen out on the wall electrodes as detailed above. The thickness of the applied layers has to yield a reasonable reservoir of material on the warm wall surface for an extended period of operation of the supersaturation cell and at the same time should not significantly disturb the electrical characteristics of the particle trap. It was found, that

a layer thickness of about 100 µm is acceptable. After applying the vapor, the particle trap is warmed to the temperature of the cold wall and after complete thermalization, the warm wall is heated further to its preset operation temperature.

Small nanoparticles of a radius of 2 – 4 nm are produced in a microwave discharge particle source by mixing a volatile metal-organic precursor gas with oxygen and a superabundance of helium and exposing the mixture to a microwave discharge (Chou and Phillips 1992; Vollath, Szabo et al. 1997; Janzen, Kleinwechter et al. 2002; Szabó 2013). The resulting nanoparticles are introduced into the vacuum system via an aerodynamic lens optimized for particles of that size (Meinen, Khasminskaya et al. 2010). They are moderated in a first He- filled octupole ion guide before singly charged particles of one polarity are directed into MICE by means of an electrostatic quadrupole deflector operating at a deflection voltage between 50 V and 250 V. In Fig. 6, we give the total number of particles in MICE as a function of duration of filling. The maximum capacity of the trap of about $8 \cdot 10^8$ particles is approached after filling it for about 60s. For the experiments described herein, the trap was operated at a total charge of about$\cdot 10^7$ particles which relates to an ion cloud radius of less than 0.5 mm. This is reached after a short filling time of 1-2 seconds. Then, the electrostatic entrance lens of MICE is closed and no more particles are admitted to the trap. Without any condensable vapor present, the particles may be stored under these conditions for more than 1000s with negligible losses. This is shown in Fig. 7 where the amount of particles in the trap is given as a function of storage time. The slight variation in stored particle amount is due to fluctuations in the particle number density of the nanoparticle source during the independent experiments.

During a typical experiment, bunches of nanoparticles are extracted from MICE at subsequently longer residence times in the trap via the exit lens and are fed into the time-of-flight (TOF) mass spectrometer. Each bunch consists of ~ 10^5 particles, so that the trap is not substantially depleted by the extraction. The TOF mass spectrometer is a home build device which employs a Daly-type detector for an efficient detection of large particles (Daly 1960). Its acceleration region is made of a modified quadrupole deflector unit. This allows interfacing the particle beam to other detectors and to further experiments. This flexibility comes at the cost of a reduced mass resolution of about m/Δm =100 which is sufficient for the application described herein. Details of this setup will be given in a subsequent publication. Any particle mass change with trapping time is attributed quantitatively to condensation processes occurring within MICE, as the flight time in the mass spectrometer is too short for significant evaporation of the particles in the mass spectrometer.

This measurement principle is demonstrated in Fig. 8, where raw mass spectra of nanoparticles exposed to a low (a) and a high (b) concentration of water vapor are displayed as a function of residence time. It is evident that in both cases the particles gain mass by the deposition and growth of ice, but the growth rate is much higher at the higher nominal supersaturation.

From such measurements, the mass growth rate of the nanoparticles can be determined as a function of the experimental parameters. In Fig. 9, we exemplarily present three different types of observed behavior. At low supersaturation (Fig. 9a) we observe an initial rapid growth of the particles that quickly levels off. At moderate supersaturation (Fig. 9b) a transition into an unlimited growth regime can be observed, while at higher supersaturation (Fig. 9c) the unlimited growth starts immediately and proceeds faster.

From the asymptotical value of the adsorption traces as shown in Fig. 9a we get the equilibrium concentration of molecules on the particle surface assuming a Langmuir-type adsorption model (Langmuir 1918) assuming sub-monolayer coverage and spherical adsorbates. We can further analyze the surface concentration using an adsorption – desorption equilibrium model (Pruppacher and Klett 2004, chap. 9.1.3). As the vapor concentration in the gas phase and the temperature are well known, the only remaining free parameter is the surface adsorption energy of vapor molecules, which can thus be deduced. In the unlimited growth regime (c.f. Fig. 9c) the sticking coefficient can be derived by comparing the measured to the theoretical mass growth rate in the gas kinetic regime (Brown, George et al. 1996; Davis 2006).

From the growth curves at intermediate supersaturation as depicted in Fig. 9b, the critical saturation and under favorable conditions the nucleation rate can be obtained. By applying classical surface diffusion nucleation theory (e.g. Keesee 1989; Pruppacher and Klett 2004; Määttänen, Vehkamäki et al. 2005) using the above determined parameters of desorption energy and nucleation rate, the effective contact angle between nanoparticle surface and the solid phase of the vapor can be deduced. Details of this analysis for different gases and nanoparticle materials will be given in forthcoming publications.

In Fig. 10, we plot the mass growth rate of water ice on silicon dioxide particles as a function of the He background gas pressure and associated Knudsen number (Kn, upper axis) under otherwise constant conditions. The curve clearly features a plateau region at lower pressure. At higher pressure, we observe a pronounced decrease in growth rate, which we attribute to the onset of the transition flow regime which is accompanied by reduced supersaturation at the trap center. It is reassuring that an area of operation can be found that allows for stable trapping of the

particles but is not influenced by the complications of the transition flow regime. For our experiments, we always limit the background gas pressure to remain in the molecular flow regime.

5.   Discussion

So far we have studied the formation of solid water ice and of carbon dioxide ice on mineral nano- particles made of iron oxide, silicon oxide and iron- silicates which are considered a proxy of meteoric dust nanoparticles found in upper planetary atmospheres. The size- material- and supersaturation- dependent nucleation and growth rates measured will be the focus of subsequent publications. Here we summarize our findings on the general applicability and limitations of this new device.

MICE proved to be a powerful tool in observing the adsorption- nucleation and growth of condensable vapors in a pressure regime compatible with molecular flow. By analyzing surface adsorption measurements, we were able to derive effective nanoparticle surface areas and surface desorption energies. In future experiments, it might be possible to study the effect of surface coatings and functional groups on these properties.

We observe that the critical vapor supersaturation needed for the nucleation of the new phase depends strongly on the type of vapor (so far, H_2O and CO_2 have been investigated). Comparing to classical heterogeneous nucleation theory, the effective contact angle between nanoparticle surface and the solid phase of the vapor can be determined. By analyzing the mass growth rate of the particles at high supersaturation, we can determine temperature- dependent sticking coefficients for the various vapors.

As detailed above, the proper functioning of the device is bound to some constraints. The pressure of the background gas needed for trapping and thermalization (He in our case) has to be much higher than the partial pressure of the vapors involved and should lie between 0.01 Pa and 0.4 Pa. The lower limit ensures sufficient friction to trap and store the particles, while the upper limit is given by the molecular flow constraint (c.f. Fig. 10). Both limits are slightly geometry- and background gas- dependent. At the same time, the concentration of vapor molecules has to be much lower than the concentration of the background gas atoms in order to ensure thermal equilibrium especially under conditions of depositional growth. At 170 K warm wall temperature and a background pressure of 0.2 Pa, the concentration of water molecules is below 1 % of the concentration of He atoms. Under these conditions, the latent heat of condensation warms the particles by at most 0.15 K. The rate of evaporation and the thickness of the condensed phase on the warm walls limit the operation over longer periods of time of the MICE at higher temperatures. At 170 K the rate of evaporation of water ice Ih in vacuo is about 4 μm/h. With an initial deposit thickness of several ten microns, this results in acceptable maximum experiment duration of 4h. At warmer temperatures, the deposit will be depleted much faster. The respective upper temperature limit for CO_2 experiments is about 90 K. Experiments are limited towards lower temperatures by the availability of vapor. Under growth conditions, the amount of deposited vapor within the experimental duration has to exceed the mass resolution of the time-of-flight mass spectrometer. These constraints define a particle temperature and saturation range which can be investigated with the device. The accessible range is given in Fig. 11 exemplarily for water vapor and for carbon dioxide.

14

So far, we have successfully applied the device to study the nucleation of water and carbon dioxide vapors on nanometer sized proxy- particles for meteoric smoke found in upper planetary atmospheres. We envision however, that similar devices may be used successfully in other fields of science ranging from catalysis to food- or drug- science. In the future, we will use MICE to extend these studies by performing an elemental analysis of the processed nanoparticles using complete laser evaporation (Wang, Zordan et al. 2006; Zordan, Pennington et al. 2010) and by studying the optical properties of growing nanoparticle systems by cavity enhanced absorption spectroscopy (Meinen, Eritt et al. 2012). We envision that tools like MICE are not only useful in atmospheric research, but that similar devices may prove useful in other fields of science ranging from catalysis to food- or drug- science.

Acknowledgments

References

Antonsson, E., H. Bresch, et al. (2013). "Free nanoparticles studied by soft X-rays." <u>Chemical Physics Letters</u> **559**: 1-11.

Bluhm, H., K. Andersson, et al. (2006). "Soft X-ray microscopy and spectroscopy at the molecular environmental science beamline at the Advanced Light Source." <u>Journal of Electron Spectroscopy and Related Phenomena</u> **150**(2–3): 86-104.

Brown, D. E., S. M. George, et al. (1996). "H_2O condensation coefficient and refractive index for vapor-deposited ice from molecular beam and optical interference measurements." <u>Journal of Physical Chemistry</u> **100**(12): 4988-4995.

Brown Jr, J. T. and F. D. Schowengerdt (1979). "Analysis of a continuous flow parallel plate thermal diffusion cloud chamber." <u>Journal of Aerosol Science</u> **10**(3): 339-348.

Chou, C. H. and J. Phillips (1992). "Plasma production of metallic nanoparticles." <u>Journal of Materials Research</u> **7**(8): 2107-2113.

Daly, N. R. (1960). "Scintillation Type Mass Spectrometer Ion Detector." <u>Review of Scientific Instruments</u> **31**(3): 264-267.

Davis, E. J. (2006). "A history and state-of-the-art of accommodation coefficients." <u>Atmospheric Research</u> **82**(3–4): 561-578.

Gumbel, J. and L. Megner (2009). "Charged meteoric smoke as ice nuclei in the mesosphere: Part 1-A review of basic concepts." Journal of Atmospheric and Solar-Terrestrial Physics **71**(12): 1225-1235.

Janzen, C., H. Kleinwechter, et al. (2002). "Size analysis in low-pressure nanoparticle reactors: comparison of particle mass spectrometry with in situ probing transmission electron microscopy." Journal of Aerosol Science **33**(6): 833-841.

Keesee, R. G. (1989). "Nucleation and Particle Formation in the Upper-Atmosphere." Journal of Geophysical Research-Atmospheres **94**(D12): 14683-14692.

Langmuir, I. (1918). "The Adsorption of Gases on Plane Surfaces of Glass, Mica and Platinum." Journal of the American Chemical Society **40**(9): 1361-1403.

Langsdorf, A. (1939). "A Continuously Sensitive Diffusion Cloud Chamber." Review of Scientific Instruments **10**(3): 91-103.

Liu, J. Y. (2005). "Scanning transmission electron microscopy and its application to the study of nanoparticles and nanoparticle systems." Journal of Electron Microscopy **54**(3): 251-278.

Määttänen, A., H. Vehkamäki, et al. (2005). "Nucleation studies in the Martian atmosphere." Journal of Geophysical Research-Planets **110**(E2).

Majima, T., G. Santambrogio, et al. (2012). "Spatial distribution of ions in a linear octopole radio-frequency ion trap in the space-charge limit." Physical Review A **85**(5).

Meinen, J., M. Eritt, et al. (2012). "Optical properties of free sub-10-nm diameter Fe2O3 nanoparticles studied by broad-band cavity enhanced absorption spectroscopy (BB-CEAS)." Applied Physics B-Lasers and Optics **108**(3): 641-647.

Meinen, J., S. Khasminskaya, et al. (2010). "Core level photoionization on free sub-10-nm nanoparticles using synchrotron radiation." Review of Scientific Instruments **81**(8).

Meinen, J., S. Khasminskaya, et al. (2010). "The TRAPS Apparatus: Enhancing Target Density of Nanoparticle Beams in Vacuum for X-ray and Optical Spectroscopy." Aerosol Science and Technology **44**(4): 316-328.

Murphy, D. M. (2007). "The design of single particle laser mass spectrometers." Mass Spectrometry Reviews **26**(2): 150-165.

Murphy, D. M. and T. Koop (2005). "Review of the vapour pressures of ice and supercooled water for atmospheric applications." Quarterly Journal of the Royal Meteorological Society **131**(608): 1539-1565.

Mysak, E. R., D. E. Starr, et al. (2010). "Note: A combined aerodynamic lens/ambient pressure x-ray photoelectron spectroscopy experiment for the on-stream investigation of aerosol surfaces." Review of Scientific Instruments **81**(1).

Nishiyama, H., M. Koizumi, et al. (2014). "Atmospheric scanning electron microscope system with an open sample chamber: Configuration and applications." Ultramicroscopy **147**(0): 86-97.

Pruppacher, H. R. and J. D. Klett (2004). Microphysics of Clouds and Precipitation. Dordrecht, Kluwer Academic Publishers.

Rapp, M. and G. E. Thomas (2006). "Modeling the microphysics of mesospheric ice particles: Assessment of current capabilities and basic sensitivities." Journal of Atmospheric and Solar-Terrestrial Physics **68**(7): 715-744.

Rogers, D. C. (1988). "Development of a continuous flow thermal gradient diffusion chamber for ice nucleation studies." Atmospheric Research **22**(2): 149-181.

Salmeron, M. and R. Schlögl (2008). "Ambient pressure photoelectron spectroscopy: A new tool for surface science and nanotechnology." Surface Science Reports **63**(4): 169-199.

Saxena, V. K. and J. C. Carstens (1971). "On the operation of cylindrical thermal diffusion cloud chambers." Journal de Recherches Atmospheriques **5**: 11-23.

Severynse, G. T. (1964). "A portable cloud nuclei counter." Journal de Recherches Atmospheriques **1**: 11-16.

Szabó, D. V. (2013). Microwave Plasma Synthesis of Nanoparticles. Microwaves in nanoparticle synthesis: fundamentals and applications. S. Horikoshi and N. Serpone. Weinheim, Wiley-VCH**: 271-310.

van der Veen, R. M., O.-H. Kwon, et al. (2013). "Single-nanoparticle phase transitions visualized by four-dimensional electron microscopy." Nat Chem **5**(5): 395-402.

Vollath, D., D. V. Szabo, et al. (1997). "Synthesis and magnetic properties of nanostructured maghemite." Journal of Materials Research **12**(8): 2175-2182.

Wang, S. and M. V. Johnston (2006). "Airborne nanoparticle characterization with a digital ion trap–reflectron time of flight mass spectrometer." International Journal of Mass Spectrometry **258**(1–3): 50-57.

Wang, S., C. A. Zordan, et al. (2006). "Chemical Characterization of Individual, Airborne Sub-10-nm Particles and Molecules." Analytical Chemistry **78**(6): 1750-1754.

Wilson, K. R., Z. Shengli, et al. (2007). "Size-dependent angular distributions of low-energy photoelectrons emitted from NaCI nanoparticles." Nano Letters **7**(7): 2014-2019.

Wu, C.-K., M. Yin, et al. (2006). "Quantitative Analysis of Copper Oxide Nanoparticle Composition and Structure by X-ray Photoelectron Spectroscopy." Chemistry of Materials **18**(25): 6054-6058.

Zordan, C. A., M. R. Pennington, et al. (2010). "Elemental Composition of Nanoparticles with the

Nano Aerosol Mass Spectrometer." Analytical Chemistry **82**(19): 8034-8038.

21

Appendix: The calculation of supersaturation in MICE

We discuss the equilibrium temperature and saturation seen by a particle completely surrounded by several (n) walls kept at temperatures $T_i (1 \leq i \leq n)$ and covered with the condensed phase of a volatile substance. The space within the walls is filled with atoms of an inert background gas, which are assumed to be much more abundant than the molecules of the vapor, but still rarefied enough to ensure free molecular flow. The notion of atoms of the background gas and molecules of the vapor is ambiguous and adopted here only for brevity; in principle both gases may either be atomic or molecular. Neglecting radiative and latent heat transfer, the particle temperature at a location $(\vec{r})$ is governed by the exchange of thermal energy with the atoms originating from the walls.

Once a stationary state has been assumed, the flux of atoms from each wall is identical. With each collision between an atom and a particle, an energy of $U_i = \alpha c_v \Delta T_i$ is exchanged; here α is the energy accommodation coefficient, c_v is the heat capacity of the atom and ΔT_i is the difference between particle temperature and the temperature of the wall that emitted the atom. Solving for a stationary particle energy budget in thermal equilibrium under the assumption of a negligible variation of α with temperature (Semyonov, Borisov et al. 1984), the position dependent particle temperature is calculated to be:

$$T_p(\vec{r}) = \sum_{i=1}^{n} F_i(\vec{r}) \cdot T_i \qquad \text{Eq. 1}$$

Here the weighting function F_i is the relative solid angle under which the wall (i) is visible from the position $\vec{r}$.

In the molecular regime, the saturation S at the particle location is given by the ratio of the flux of condensable vapor molecules at the particle location relative to the flux of molecules the particle would experience when being in equilibrium with the condensed phase at the particle temperature.

$$S(\vec{r}) = \frac{J_{vap}(\vec{r})}{J_{vap,sat}(T_p)}$$ Eq. 2

The equilibrium flux over the condensed phase is

$$J_{vap,sat}(T_p) = \frac{p_{sat} v_{th}}{4 k_B T_p}$$ Eq. 3

, where p_{sat} is the saturation vapor pressure and $v_{th} = \sqrt{8 k_B T_p / \pi m}$ is the mean thermal velocity of the vapor phase molecules of molecular mass m at the particle temperature T_p. The total flux of condensable vapor molecules towards the particle surface is given by the sum of the fluxes from the walls weighted with their respective weighting function.

$$J_{vap}(\vec{r}) = \sum_{i=1}^{n} F_i(\vec{r}) \cdot J_{vap}(T_i)$$ Eq. 4

Equations 1 and 4 show that in the molecular regime temperature and saturation conditions are determined by the solid angle weighting functions. In contrast, in the continuum case the conditions are governed by the temperature and concentration gradients.

In this manuscript we deal with two walls only, i.e. the warm wall at temperature T_w with weighting function F_w and the cold wall at temperature T_c and weighting function $(1 - F_w)$.
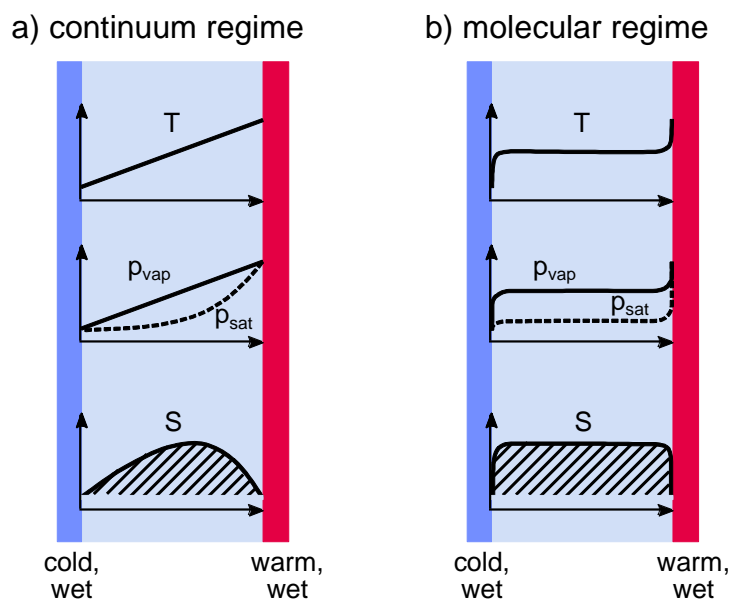
Figure 1 Schematic representation of a supersaturation chamber (a) diffusion cloud chamber, (b) free molecular flow cloud chamber. The slightly rounded edges of all curves in (b) reflect the fact that the molecular flow assumption breaks down for infinitely sized plates.
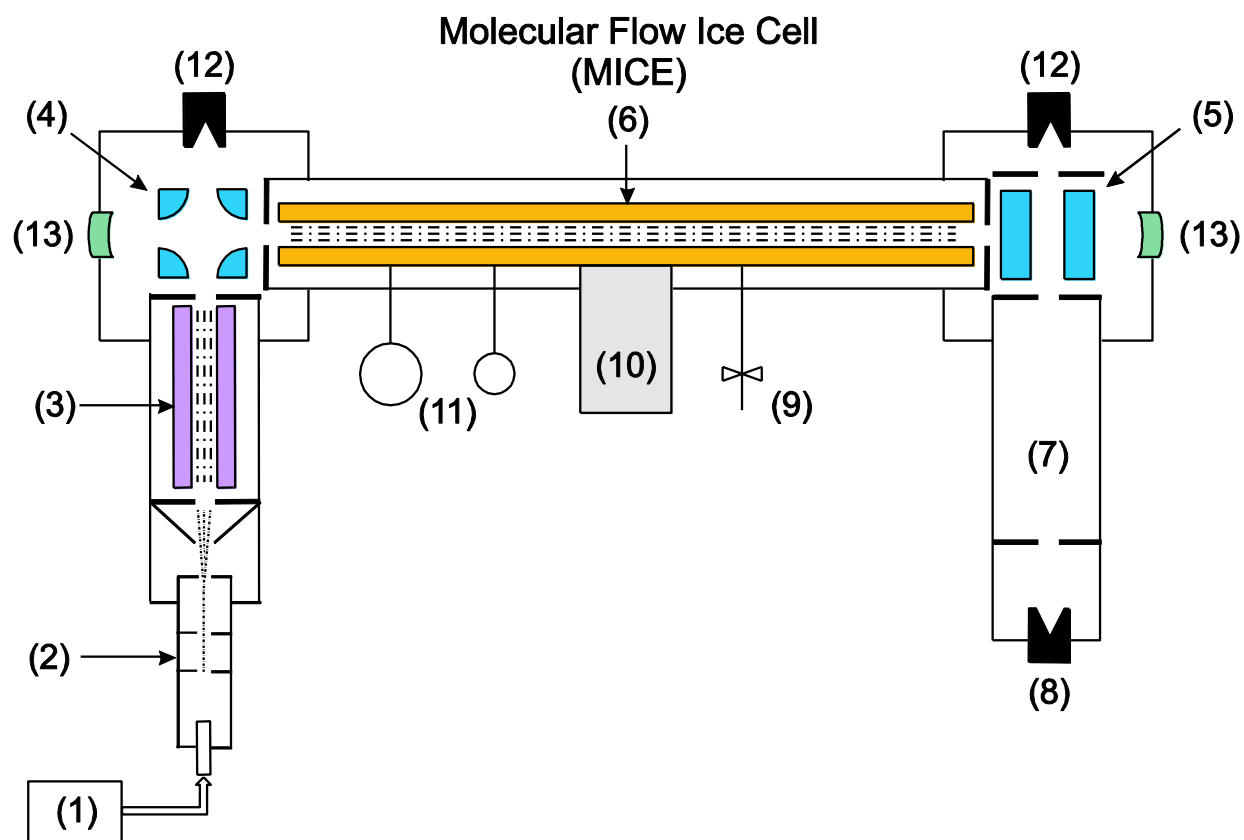
Figure 2 Schematic setup of the TRAPS apparatus including MICE. The labeled parts are: (1*)* nanoparticle source, (2*)* aerodynamic lens, (3) octupole ion guide, (4*)* quadrupole deflector, (5*)* quadrupole deflector rotated by 90° into plane, (6) MICE, (*7)* wide range time-of-flight mass spectrometer, (8*)* Daly-type nanoparticle detector, (9*)* mass flow regulated gas inlet, (10) cryo stage, (11) residual gas analyzer and pressure gauge, *(12)* Faraday cup detector, (13*)* high reflectivity optical cavity mirror.
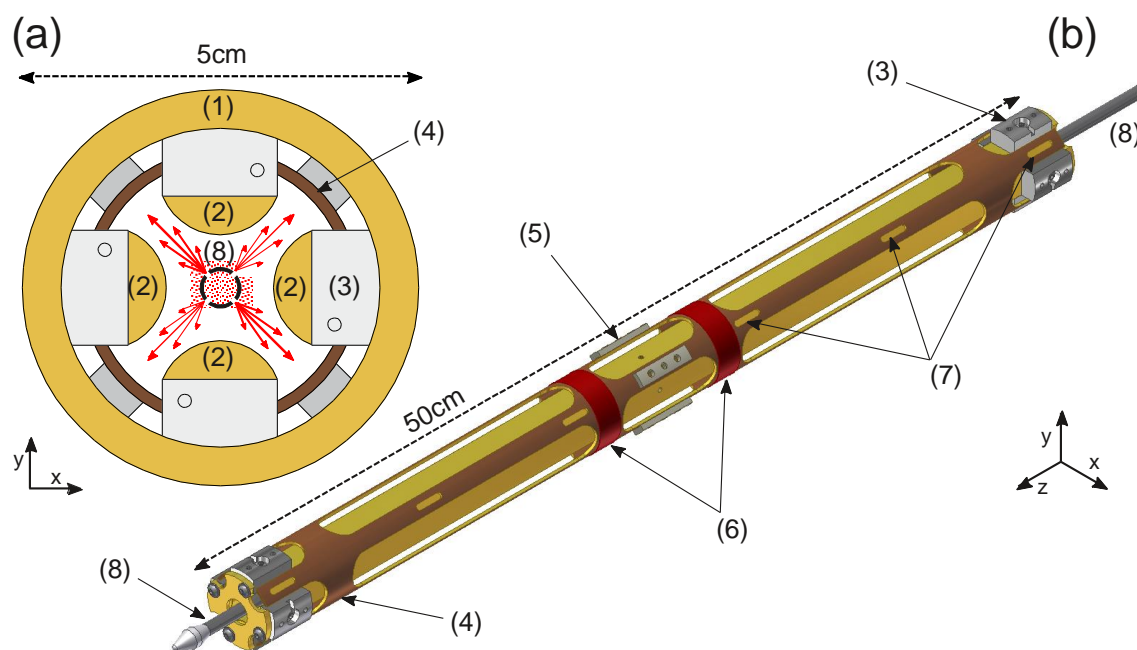
Figure 3 Design of MICE. Radial cross section shown in panel (a) and perspective view on reduced scale with cooling tube omitted in panel (b). The labeled parts are: (1) cooling tube, (2) quadrupole ion trap electrodes, (3) SHAPAL spacers, (4) heated electrode on ground potential, (5) PEEK spacers, (6) heating foils, (7) temperature sensor cavities, (8) retractable condensable vapor applicator tube.
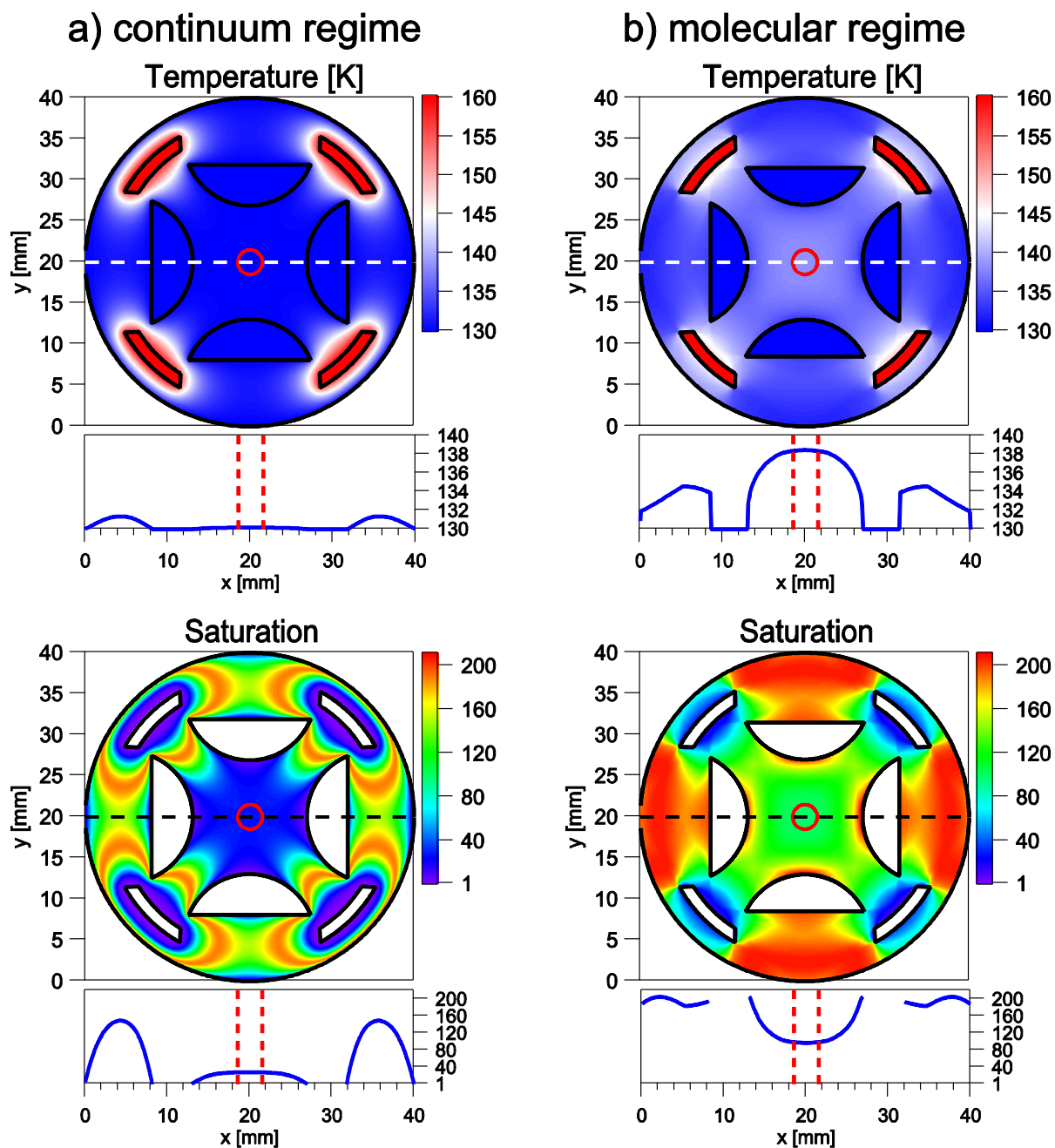
Figure 4 Calculated radial temperature and saturation profiles of MICE (a) in the viscous and (b)

in the molecular regime for selected temperatures of 130 K (cold electrodes) and 160 K (warm

27

electrodes). Horizontal cross sections are shown right below each plot. Vertical dashed lines and

the central dashed circles indicate ion cloud extent during typical operation conditions.
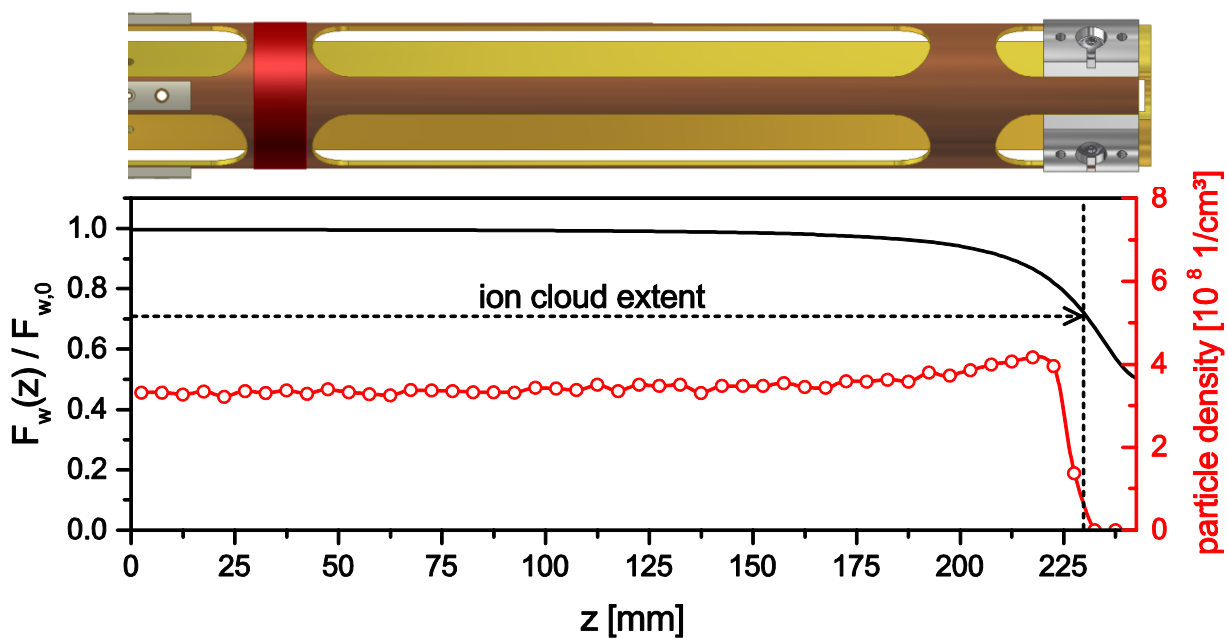
Figure 5 Warm surface weighting function F_w (solid line, left scale) and particle density from a

SIMION simulation (circles, right axis) along the axis of the MICE. For symmetry reason only

one half of the device is shown.
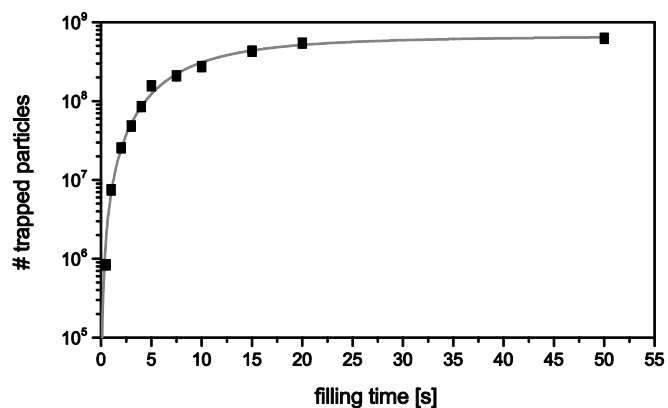
Figure 6 Total number of particles stored in the Ion trap as function of the filling time for $m=1.8 \cdot 10^5$ u SiO_2 particles with $V_{rf}=950$ V and f=50 kHz. The trap capacity for SiO2 particles of the selected mass is about $8 \cdot 10^8$ particles which corresponds to an average particle density within the ion cloud of about $4.5 \cdot 10^8$ 1/cm³.
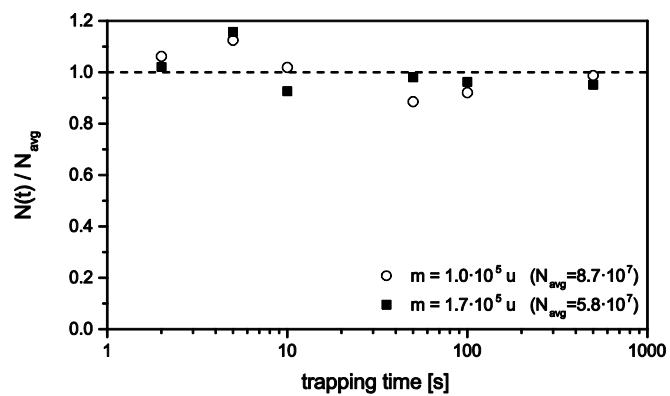
Figure 7 Trapping efficiency of the MICE. Shown is the number of particles stored in the ion trap normalized to the average as a function of trapping time for two selected particle masses.

ACCEPTED MANUSCRIPT
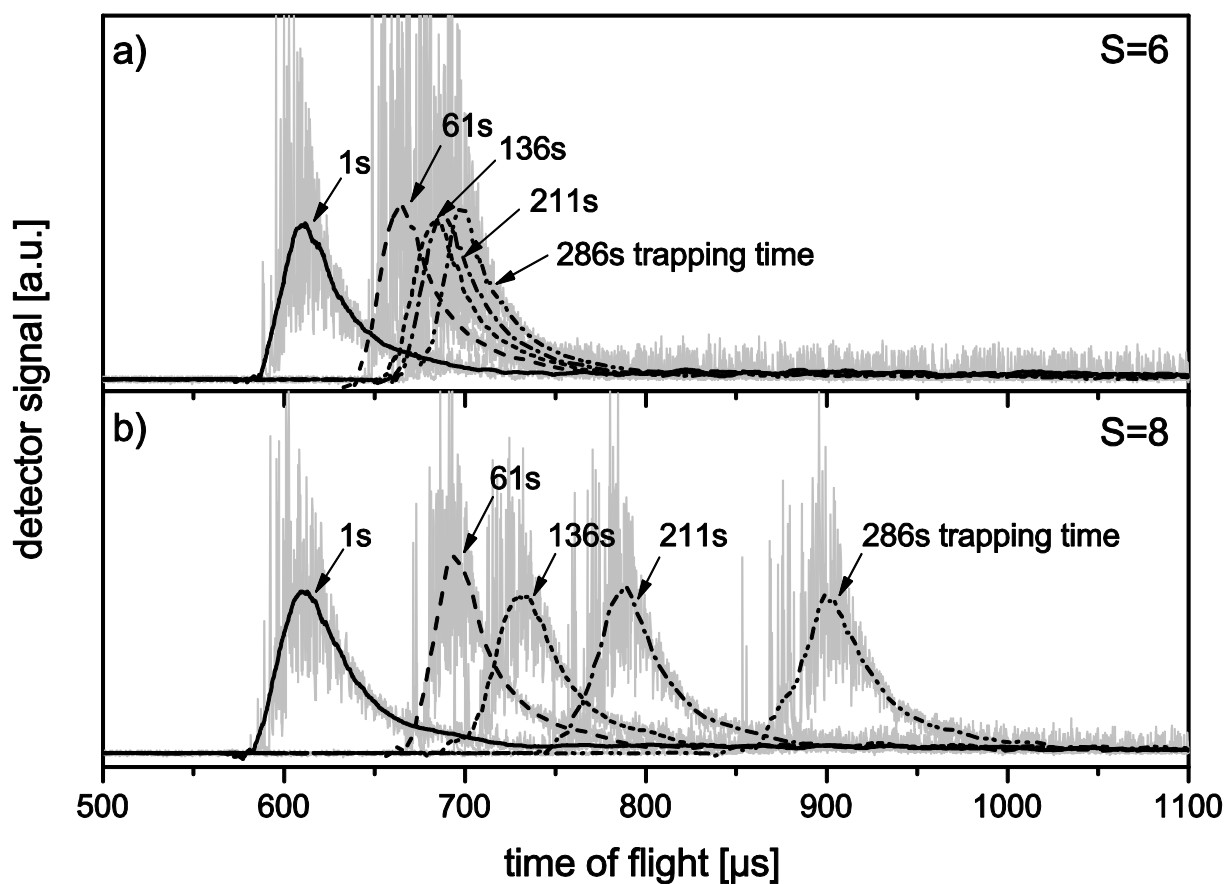
Figure 8 Time-of-Flight spectra for silicon oxide particles at water vapor growth conditions in the MICE for five different trapping times. Raw data in gray overlayed with smoothed curves using 3rd order Savitzy-Golay filter.
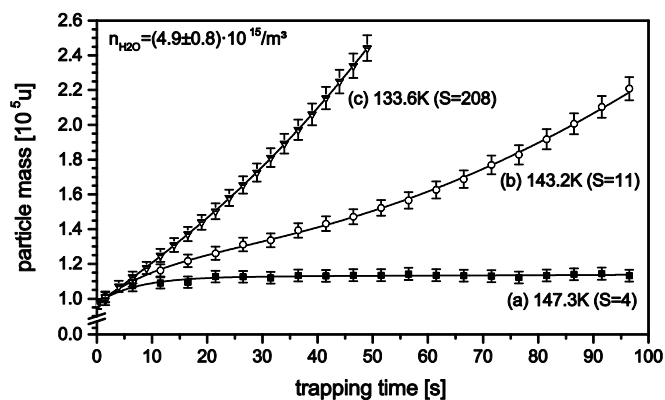
Figure 9 Deposition growth of water vapor on silicon oxide particles measured at three different particle temperatures and saturations at a constant water vapor concentration. Solid lines are fits using a linear combination of exponential decay and 2nd order polynomial.
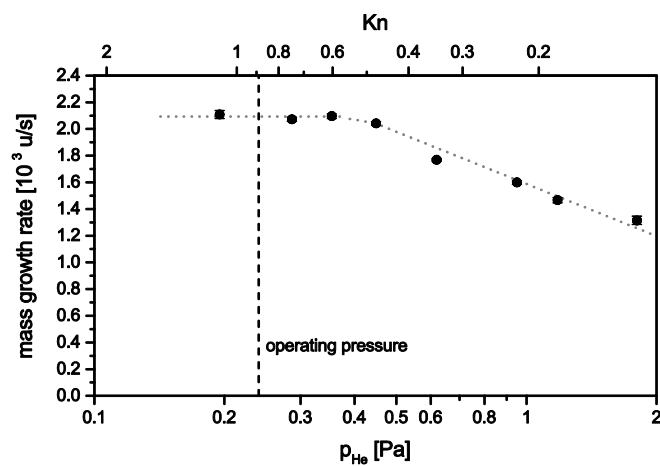
Figure 10 Water vapor deposition rate on silicon oxide particles as function of Helium background gas pressure (lower scale) and corresponding Knudsen number (upper scale).
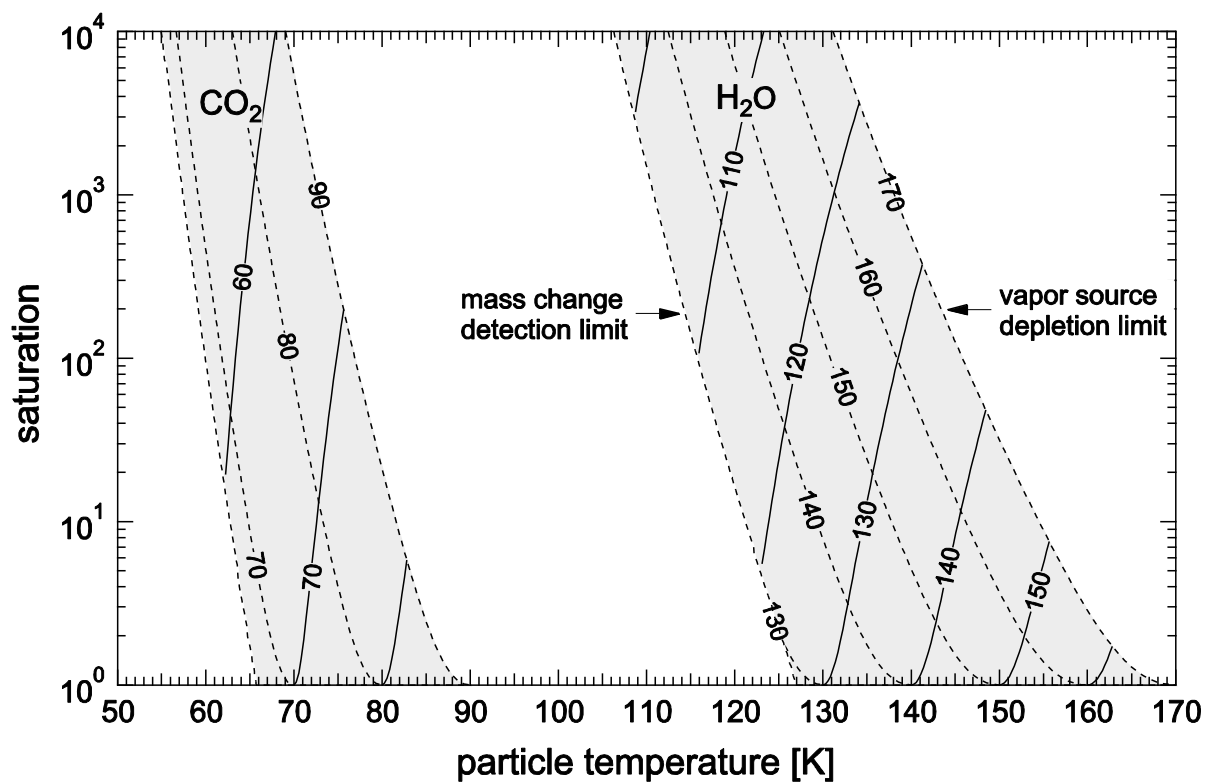
Figure 11 Operation regimes of the MICE for water vapor and carbon dioxide. Isothermals of

the cold wall (solid lines) and of the warm wall temperature (dashed lines) with numbers given in

degree Kelvin.